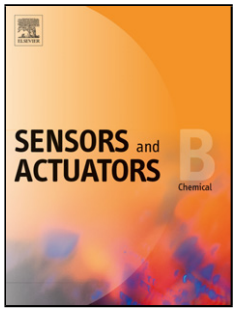

Title: Enhanced photostability and sensing performance of graphene quantum dots encapsulated in electrospun polyacrylonitrile nanofibrous filtering membranes

Authors: Virginia Ruiz, Ana Pérez-Marquez, Jon Maudes, Hans-Jürgen Grande, Nieves Murillo

PII: S0925-4005(18)30359-9
DOI: https://doi.org/10.1016/j.snb.2018.02.081
Reference: SNB 24176

To appear in: *Sensors and Actuators B*

Received date: 14-9-2017
Revised date: 8-2-2018
Accepted date: 9-2-2018

Please cite this article as: Virginia Ruiz, Ana Pérez-Marquez, Jon Maudes, Hans-Jürgen Grande, Nieves Murillo, Enhanced photostability and sensing performance of graphene quantum dots encapsulated in electrospun polyacrylonitrile nanofibrous filtering membranes, Sensors and Actuators B: Chemical https://doi.org/10.1016/j.snb.2018.02.081

Enhanced photostability and sensing performance of graphene quantum dots encapsulated in electrospun polyacrylonitrile nanofibrous filtering membranes

Virginia Ruiz[a,*], Ana Pérez-Marquez[b], Jon Maudes[b], Hans-Jürgen Grande[a] and Nieves Murillo[b,*]

[a] CIDETEC, Paseo Miramón 196, E-20014 Donostia-San Sebastián, Spain.

[b] TECNALIA, Paseo Mikeletegi 2, E-20009 Donostia-San Sebastián, Spain

Graphical Abstract

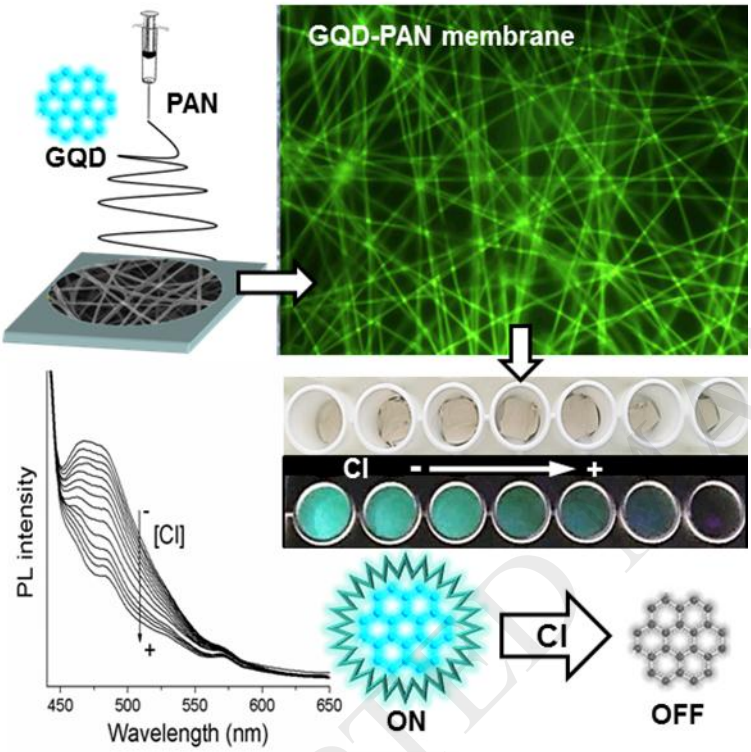

Highlights

- Graphene quantum dots/polyacrylonitrile membranes were prepared by electrospinning
- GQD-PAN filters are turn-off fluorescence sensors for free chlorine detection
- Membranes have fast sensing response to chlorine concentration (10-600 μM range)
- Filters show high sensitivity (DL=2 μM detection limit), reproducibility (< 5% RSD) and selectivity
- Filters sensing response was stable after months immersed in buffer solutions

*Corresponding author. E-mail: vruiz@cidetec.es; nieves.murillo@tecnalia.com

Abstract

We report a method to encapsulate graphene quantum dots (GQD) in polyacrylonitrile (PAN) nanofibrous membranes to manufacture robust filtering membranes by electrospinning. GQD-PAN

membranes with different nanofiber diameter were prepared tuning the electrospinning parameters, all exhibiting the characteristic fluorescence fingerprint of the GQD probes. The photoluminescence (PL) stability of GQD embedded in the PAN fibers was significantly enhanced with respect to that of water dispersed GQD luminescent probes. The PL of GQD-PAN filtering membranes showed remarkable time stability, both stored dry and immersed in phosphate buffer solutions (PBS), as well as exposed to continuous light irradiation. However, the PL intensity of GQD-PAN membranes was irreversibly quenched by highly oxidant free chlorine solutions. Thus, electrospun GQD-PAN membranes exhibited excellent performance as turn-off fluorescence sensing platforms for free chlorine detection in PBS 0.1 M pH 7. The analytical performance of GQD-PAN membranes was comparable to that of GQD solutions with optimal concentrations, displaying a fast (no need of incubation time) and linear response to chlorine concentration in the 10-600 μM range, a low detection limit of 2 μM, high sensitivity, reproducibility and selectivity. Moreover, the sensing performance of the membranes was very stable after being immersed in PBS for months, outperforming the stability of GQD solutions.

Keywords: graphene quantum dots; nanofibers; membranes; electrospinning; fluorescence sensor; chlorine detection

1. Introduction

Graphene quantum dots (GQD) are graphene sheets smaller than 100 nm that are attracting enormous interest in view of their fascinating and easily tunable electronic and optical properties [1,2]. GQD are regarded as versatile fluorophores due to their size- and composition-dependent emission that can be tailored by the synthetic method [3]. Moreover, depending on the preparation method GQD may exhibit outstanding luminiscence properties such as high photostability against bleaching and blinking in addition to biocompatibility, excellent solubility and lower toxicity than semiconductor quantum dots [4]. All these attractive features have triggered investigation of GQD for applications in different fields such as lighting, bioimaging, photovoltaics, energy conversion and storage,

catalysis or sensing [5-9]. Among them, GQD have attracted tremendous attraction in the analytical field as sensing probes for diverse environmental and biological applications [10,11]. Based on different GQD properties and sensing mechanisms, GQD have been applied in electronic, electrochemical, electrochemiluminescence and photoluminescence (PL) sensors [9]. In "turn-off" PL sensors, GQD fluorescence is selectively quenched by the analyte. Fluorescence quenching is based on photo-induced electron transfer from excited GQD to the analyte. By tailoring the bandgap and functional groups in GQD, selectivity towards detection of different target analytes has been achieved, such as Hg^{2+} [12], Fe^{3+} [13], Cu^{2+} [14], Ni^{2+} [15], ClO^{-} [16], glucose [17], fructose [18], melamine [19], among others. In most studies, GQD are used as soluble fluorescent probes for turn-off selective sensing co-dispersed with the target analyte.

On the contrary, the development of PL sensing platforms based on GQD confined to surfaces is comparatively scarce despite being more practical from the application's viewpoint. There are several studies reporting incorporation of GQD in filtration membranes by different methods (covalent bonding, interfacial polymerization, layer-by-layer assembly) to produce membranes with bactericidal properties [20], enhanced antifouling performance [21] and chlorine resistance [22]. In the field of sensors, there are just few examples of surface-confined GQD-based PL sensing platforms. Thus, GQD-chitosan-creatinine mixtures were deposited on silica slides and the resulting fluorescent films were applied to detect picric acid in water by measuring film PL quenching [23]. A solid fluorescent sensor for selective detection of Fe^{3+} was also developed by adsorbing GQD on a polystyrenic anion-exchange resin [24]. Similarly, a fluorescent polyacrylonitrile membrane for Fe^{3+} detection was reported where carbon dots were encapsulated in a mesoporous silica coating around the membrane fibers [25]. GQD were also chemically bonded to nylon membranes to yield fluorescent membranes with excellent sensing performance for Cr^{6+} detection [26].

All these studies highlight the preservation of GQD intrinsic fluorescence and sensing ability after immobilization onto different surfaces. However, the preparation methods involve post-deposition of GQD on the host matrix or complex encapsulation methods. Developing strategies for

one-step integration of GQD during membrane preparation would contribute to large-scale and high-throughput manufacturing of the sensing membranes. In this regard, electrospinning represents an attractive and versatile strategy to embed GQD in filtering membranes as it enables control over membrane fiber diameter, thickness, good mechanical strength, high porosity and surface area per unit mass, areal weight control, GQD loading, etc [27,28]. Electrospinning represents a low-cost solid route to manufacture filtering membranes with sensing properties. As an example, Zhang et al immobilized GQD into a nanofibrous membrane by electrospinning water-soluble GQD and polyvinyl alcohol, fabricating a fluorescence and electrochemical biosensing platform for H_2O_2 detection [29].

On the other hand, determination of free residual chlorine in water is very important as its concentration should be strictly controlled and maintained at appropriate level, because of its relevance as quality control index. Too high concentration may lead to production of harmful trihalomethanes by reaction with organic matter present in water [30]. On the other hand, too low concentration may not ensure the microbiological level of disinfection required to keep water clean [31]. The different chlorine-based oxidizing compounds (Cl_2, HClO, ClO^-) accounting for the total amount of free residual chlorine in water are extensively used as disinfectants in water treatment, hence the need of efficient analytical methods to monitor their concentration in water. Common analytical techniques for selective determination of free chlorine include different spectrophotometric, electrochemical and liquid chromatographic methods, each having different drawbacks [32, 33, 34]. The main concern related with analytical methods for free chlorine measurement is the time-delay due to water travel from chlorine dosage station to the distribution networks and measurement points. Under this complex scenario, low cost, selective and robust sensors to monitor free chlorine are needed.

In this paper, we report the successful incorporation of GQD into electrospun polyacrylonitrile (PAN) membranes, demonstrating the excellent and stable performance of GQD-PAN filtering membranes as turn-off fluorescent sensing platforms for selective and sensitive detection of free

chlorine in water. The capacity of strongly oxidizing chlorine to quench the luminescence of dispersed GQD probes has been previously demonstrated [16], which is the fundamental sensing principle of the nanofibrous filtering membrane developed by the authors. Here we have produced PAN membranes containing GQD by one-step electrospinning solutions of both components with very homogeneous GQD distribution across the membrane volume. The resulting fluorescent GQD-PAN membranes have proven to be very sensitive fluorescence sensing platforms for selective determination of free chlorine in water. Moreover, we will demonstrate that GQD exhibit more stable luminescence emission protected by the PAN fibers than dispersed in water. As a result, the analytical performance of GQD-PAN membranes remained very stable after months immersed in aqueous buffer solution.

2. Materials and methods

2.1. Reagents and materials

NaCl, KCl, $NiCl_2.6H_2O$, $ZnCl_2$, $CuCl_2.2H_2O$, $MnSO_4$ and $CoCl_2.6H_2O$ purchased from Scharlau. Stock NaClO (10%) solution, $Cd(ClO_4)_2$, $FeCl_2.4H_2O$, $MgCl_2.7H_2O$, $CaCl_2$, $AgNO_3$, $Pb(ClO_4)_2$, $Hg(ClO_4)_2$, KH_2PO_4, Na_2HPO_4, pyrene, ammonia, hydrazine hydrate, polyacrylonitrile (PAN) with molecular weight M_w = 150.000 g.mol^{-1} and *N*,*N*-dimethylformamide (DMF) were purchased from Sigma Aldrich (Spain) and $FeCl_3.6H_2O$ from Panreac. All chemicals were of analytical grade and used without further purification. All solutions were prepared with ultrapure water of Synthesis A10 from Millipore (18Ω.cm) (Massachusetts, USA). The concentration of free chlorine in the stock solution was determined by iodometric titration.

2.2. Instrumentation

GQD-PAN nanofibrous filtering membranes were prepared using a custom-made needle electrospinning apparatus. The NE-1000 dosage pump speed range available is 0.73 µL/h to 2100 mL/h. The applied voltage between needle and collector (30 kV) was generated using a high voltage

power supply (model AU-30R1-L from Matsusada Precision Inc). The needle – collector configuration was vertically oriented (supporting information, Figure S1). The electrospinning setup is equipped with humidity control until 20% RH.

The morphology of nonwoven GQD-PAN nanofibrous membranes was studied by scanning electron microscopy (JSM 5910-LV JEOL) to determine electrospun nanofiber diameter, homogeneity and defect concentration. The average diameter of the GQD-PAN nanofibers in the filtering membrane was determined using the Image-J image processing program [35]. GQD-PAN membrane photoluminescence was characterized using a BX51 fluorescence microscope (OLYMPUS) equipped with a Color View III camera and an U-LH100HG mercury excitation source with λ = 450 - 495 nm. Absorption and fluorescence spectra were measured with a Jasco V-570 UV-VIS-NIR spectrophotometer and a Varian Cary Eclipse fluorescence spectrophotometer, respectively. TEM images of GQD on carbon-coated copper grids were taken using a TECNAI G2 20 TWIN (FEI) transmission electron microscope, operating at an accelerating voltage of 200 KV in a bright-field image mode. AFM images of GQD on mica substrates were obtained in tapping mode at room temperature using a scanning probe microscope (Molecular Imagings PicoScan) equipped with a Nanosensors tips/cantilever, at a resonance frequency of 330 kHz and a spring constant of about 42 N/m, with a tip nominal radius lower than 7 nm. XPS measurements were performed in a SPECS Sage HR 100 spectrometer with a non-monochromatic X-ray source (Magnesium Kα line of 1253.6 eV energy and a power applied of 250 W) and calibrated using the $3d_{5/2}$ line of Ag with a full width at half maximum (FWHM) of 1.1 eV. Measurements were made in an ultra-high vacuum chamber at a pressure around 8×10^{-8} mbar. Raman spectra of freeze-dried solutions were measured with a Confocal Raman Voyage spectrophotometer (BWTEK, USA) at an excitation wavelength of 532 nm.

2.3. Synthesis of GQD

GQD were synthesized according to a method reported elsewhere [36]. Briefly, in a typical procedure pyrene (1g) was nitrated into 1,3,6-trinitropyrene in 65% wt. HNO_3 (80 mL) under refluxing and

stirring for 16h. After cooled to room temperature, the mixture was diluted with deionized (DI) water and filtered through a 0.22 μm nylon membrane. Part of the resultant 1,3,6-trinitropyrene (1 g) was dispersed by ultrasonication in a DI water solution (0.1 L) containing 0.2 M ammonia and 1.5 M hydrazine hydrate for 1 h. The suspension was transferred to a teflon-lined autoclave and heated at 200 ºC for 8 h. After cooled to room temperature, the GQD solution was filtered through a 0.22 μm nylon membrane to remove insoluble carbon product, and further dialysed in a dialysis bag (retained molecular weight: 3500 Da) for 1 day to remove salt and small molecules.

2.4. Preparation of GQD-PAN electrospun nanofibrous membranes

Dry GQD were dispersed in DMF using magnetic stirring for 1 hour and GQD loading was 0.5 wt% referred to the polymer weight. PAN pellets were dissolved at 10 and 12 wt.% in the GQD/DMF dispersion by magnetic stirring for 24h at room temperature. The dispersions were loaded into 10 mL plastic syringes and dispensed at a flow rate of 0.63 mL/h. The applied voltage was kept constant at 15 kV and the distance between the needle and the collector was 240 cm during the electrospinning process. All electrospinning experiments were carried out under humidity control, with 50 % relative humidity at approximately 20 ºC. After the stable jet formation, electrospun GQD-PAN nanofibrous membranes were collected on aluminium foil, which was removed for membrane characterization.

Electrospun filtering membranes prepared from PAN 12 wt% and GQD 0.5 wt% in DMF solution were referenced as GQD-PAN12 while membranes prepared from PAN 10 wt% and GQD 0.5 wt% in DMF solution were named as GQD-PAN10. As control, electrospun GQD-free PAN nanofibrous membranes were manufactured to confirm lack of interference between GQD and polymer fluorescence.

2.5. Fluorescence measurements of dispersed GQD and GQD-PAN membranes

Fluorescence measurements were done in 96-well fluorescence plates, placing either GQD solutions or small pieces (4 mm x 4 mm) cut from GQD-PAN electrospun membranes at the bottom of the wells. Fluorescence spectra were recorded at a scan rate of 10 nm/s and a 5 nm slot width, both for

excitation and emission. Fluorescence quenching by the different analytes was measured at the maximum emission wavelength of the GQD-PAN membranes, 478 nm, at an excitation wavelength of 420 nm. The background fluorescence of GQD-free PAN electrospun membranes at the excitation wavelength (420 nm) was subtracted from the spectra on GQD-PAN membranes. Blank PL measurements were done with the GQD-PAN membrane immersed in 0.1 M phosphate buffer pH 7 (PBS) to rule out photodegradation. The fluorescence quenching effect of different chlorine concentrations on each type of GQD-PAN membrane was investigated by adding aliquots of NaClO in PBS onto wells containing different pieces of each membrane immersed in PBS. Three replicates were measured for each chlorine concentration. Fluorescence measurements both for dispersed GQD and GQD-PAN membranes were done immediately after adding the test solutions without any incubation time.

3. Results and discussion

3.1. Characterization of GQD and GQD-PAN membranes

The size and thickness of GQD synthesized by hydrothermal condensation of 1,3,6-trinitropyrene were examined by TEM and AFM. TEM and AFM images (Fig. 1a and b) reveal that GQD are very uniform in terms of lateral size and thickness, with an average size of 2.7 ± 0.4 nm and height of 1.5 ± 0.4 nm, indicating that most GQD were composed of 2-5 layers. A full characterization of comparable GQD samples by Raman, XPS and FTIR spectroscopies was carried out in previous studies [26, 37]. Both XPS and FTIR spectroscopy (supporting information, Fig. S2 and S3A) corroborated that GQD have amine and hydroxyl groups originating from the precursor and the media (hydrazine and ammonia) used in the condensation reaction. The chemical composition of the GQD estimated from the XPS survey spectrum indicates 71.1 at.% C, 18.2 at.% O and 10.7 at.% N contents. That is, the O/C atomic ratio for GQD (0.26) falls in the range of values reported for different types of reduced graphene oxides (0.15-0.28) and is considerably lower than graphene oxide ratios (0.4-0.6) [38].

The optical properties of GQD were investigated by UV-visible absorption and fluorescence spectroscopy (supporting information, Fig. S4). The UV-visible absorption spectrum (black line in Fig. S4a) exhibits three well-defined absorption bands located at 250, 290 and 400 nm, which can be assigned to the π-π* transition of the aromatic sp^2 domains and electronic transitions between energy levels of surface states arising from the functional groups [7]. The PL excitation spectrum (blue line in Fig. S4a) features three intense bands at 260, 308 and 418 nm, in good agreement with the corresponding UV-vis absorption bands. The most intense PL emission (red line in Fig. S4a), centered at 498 nm, is obtained with an excitation wavelength of 420 nm. However, the PL emission is excitation-dependent; when the excitation wavelength is increased from 340 to 460 nm the PL emission peak slightly shifts to longer wavelengths (from 475 to 505 nm) and at long excitation wavelengths the PL intensity decreases sharply (Fig. S4b). This excitation-dependent PL emission has been commonly observed in GQD and has been ascribed both to excitation of different sized GQD or conjugated sp^2 carbon domains in the GQD carbon network [39].

Next, PAN and GQD-PAN electrospun membranes were characterized. As shown in Figure 2a and 2b, GQD-PAN membranes exhibit a pale yellow coloration compared with white PAN electrospun membranes. Photoluminescence of GQD-PAN10 and GQD-PAN12 electrospun membranes, with 2.83 and 2.00 $\mu g/cm^2$ of GQD respectively, was investigated using a fluorescence microscope. GQD emission is perceptible in the electrospun nanofibrous membranes upon excitation with a UV-vis light source (450 nm - 495 nm), as seen in Figure 2c (sunlight) and 2d (UV-vis light). A very homogeneous distribution of GQD was observed across the whole nanofiber area in the nanofibrous membranes. From fluorescence microscopy observation, the spinnability of PAN, GQD-PAN10 and GQD-PAN12 solutions was confirmed due to the absence of defects.

The absence of defects and nanofiber morphology were further examined by Scanning Electron Microscopy (SEM), for both GQD-PAN10 and GQD-PAN12 filtering membranes (Figure 3). The average nanofiber diameter was calculated using Image-J image analysis program. Approximately 250 measurements were used to estimate the nanofiber average diameters and distribution (Figure 3c

and 3d). The average nanofiber diameter increased from 595 nm (GQD-PAN10) to 762 nm (GQD-PAN12) when PAN content in the initial precursor solution increased by 2 wt%. A similar change was observed in the GQD-free PAN nanofibrous membranes, where the average nanofiber diameters increased from 458 nm to 553 nm in membranes electrospun from 10 wt% and 12 wt% PAN solutions in DMF, respectively. This average diameter growth is directly related to an increase in viscosity of the precursor solution [28]. GQD addition into the PAN solution, even at a very small content of 0.5 wt.%, further increases the viscosity of the electrospinning solution and, as consequence, nanofiber diameters grow compared to GQD-free PAN solutions. A comparable growth was noted for both samples, GQD-PAN12 and GQD-PAN10.

The PL emission spectra of PAN and GQD-PAN electrospun membranes as well as water dispersed GQD were measured by fluorescence spectroscopy. The PL emission spectra of GQD-PAN membranes and water dispersed GQD at a same excitation wavelength (420 nm) are compared in Fig. 4 together with the spectrum of a GQD-free PAN electrospun membrane. At this excitation wavelength, PAN has a considerable emission, with a clear shoulder at 480 nm that is also well-resolved in the spectra of GQD-PAN membranes together with a band at 466 nm. The spectra of GQD-PAN membranes after subtracting the contribution of PAN emission at this wavelength (Fig. 4) exhibit a well-defined band centered at 478 nm corresponding to the emission from the GQD. PL emission of GQD in PAN membranes is blue-shifted with respect to that of water dispersed GQD, whose band is centered at 498 nm. In contrast, no emission shift was noted in our previous work where GQD were immobilized at the surface of a nylon membrane instead of embedded within the PAN fibers in the membrane [26]. As it is well known that GQD PL emission is largely affected by the environment [40], the blue shift is most likely caused by interactions between functional groups of GQD and the PAN host matrix, as has also been reported for GQD embedded in other matrices such as polystyrene [24] and silica [25]. The considerable broadening of the nitrile stretch band (at 2242 cm^{-1}) in the FTIR spectra of GQD-PAN membranes (supporting information, Fig. S3C) suggests the formation of hydrogen bonds between nitrile groups of PAN and hydroxyl and amine groups of

GQD [41]. Moreover, the red shift of C=C stretch bands (at 1590 and 1504 cm^{-1}) in GQD-PAN membranes may also point at π-π interactions between sp^2 carbon domains of GQD and nitrile groups of PAN [42].

Electrospun GQD-PAN membranes with different fiber diameter exhibit comparable fluorescence intensity, as expected in view of their similar overall GQD content (2.00 – 2.83 $\mu g/cm^2$). Moreover, the emission intensity at 480 nm determined from the PL spectra of 10 different pieces cut out of each membrane (supporting information, Fig. S5 and S6) has a relative standard deviation (R.S.D.) of 6.5% (GQD-PAN12) and 10.1% (GQD-PAN10), demonstrating that GQD loading across the whole membrane area (300 cm^2) was very homogeneous, as also observed by fluorescence microscopy.

3.2. Luminescence stability of GQD and GQD-PAN membranes

Before assessing the performance of GQD-PAN membranes as fluorescent sensing platforms, we examined the stability of GQD PL intensity embedded in the PAN fibers. The time evolution of PL intensity at 478 nm (λ_{exc} = 420 nm) of a dry GQD-PAN10 membrane measured at different days over a 2-month period is shown in Fig. 5a. The plotted values of relative PL intensity (F) with respect to the initial emission (F_0) are the average of 5 replicates from different pieces of membrane. As can be seen, a negligible F/F_0 decrease (1%) was noted after 2 months for the GQD luminescent probes embedded in the dry GQD-PAN membrane. On the contrary, a substantial PL emission loss (35%) was observed for GQD aqueous solution (0.015 mg/mL) after 2 months stored at 4º C. Although GQD exhibit high intrinsic PL photostability, when dispersed in solution media they eventually tend to coalesce and precipitate, hence the long-term lower luminescence. That is, encapsulating the GQD luminescent probes into the PAN nanofibrous membrane by electrospinning not only preserves their PL properties but also leads to enhanced long-term photostability. The improved stability of embedded GQD probes may result from passivation of their surface functional groups due to

formation of hydrogen bonds with the PAN host matrix, which also prevents their leakage from the membrane (vide infra).

Next, the photostability of GQD-PAN membranes under continuous irradiation with a fluorescent tube lamp (22W) was investigated. Fig. 5b shows time evolution of relative PL intensity values (F/F_0) at 478 nm (λ_{exc} = 420 nm) obtained as the average of 5 replicates from different pieces of a dry GQD-PAN12 membrane. After 2h of continuous exposure, most of the initial emission intensity was retained (96%), as evidenced by the photographs of the membrane taken under UV light (365 nm) before and after the photostability test (Fig. 5b), showing an unaltered bright cyan emission. With the aim of applying GQD-PAN membranes as turn-off PL detection platforms for free chlorine, we explored their stability immersed in phosphate buffer solution (PBS) 0.1 M pH 7. As explained in next section, controlling the solution pH is crucial as it will affect both GQD PL intensity and the form of free chlorine in water. Several pieces (N=5) of GQD-PAN membranes with the two fiber diameters were immersed in PBS 0.1 M pH 7 inside the fluorescence plate wells and their PL spectra measured on different days over a period of 2 months. The average relative PL intensity values (F/F_0) at 478 nm (λ_{exc} = 420 nm) for the two membranes at different immersion times are compared in Fig. 5c. The soaked membranes were stored in the dark at room temperature between PL measurements. In order to rule out a possible emission from GQD leaking out of the membrane, the PL of the solution after 1 day in contact with several membrane pieces was measured, which displayed negligible emission, corroborating the high stability of GQD inside the PAN nanofiber. As in the case of dry GQD-PAN membranes, the evolution of PL intensity with immersion time (Fig. 5c) highlights a higher long-term stability of GQD luminescence when encapsulated in PAN fibers than as dispersed probes. Improved PL stability, although over much shorter timescales, was also reported for carbon dots immobilized in silica [25] and was also ascribed to formation of hydrogen bonds between the luminescent probes and the silica host matrix. Here GQD encapsulated in the PAN membrane with smaller diameter fibers (595 nm) and higher GQD content (2.8 $\mu g/cm^2$), that is, GQD-PAN10 sample exhibit more stable emission than GQD-PAN12 nanofiber membrane. Wang et al. [43] demonstrated

the influence of nanofiber diameter in pore size for electrospun polyurethane filtering membranes, where pore volume increased with nanofiber diameter, resulting in higher hydrophobicity of the electrospun membrane surface. A lower GQD content in the GQD-PAN12 membrane, together with a higher nanofiber diameter and hydrophobicity could be responsible for the small PL decay (7%) compared to the GQD-PAN10 sample. The lower hydrophobicity and higher GQD content of GQD-PAN10 membrane may give rise to more interactions between acrylonitrile groups and GQD functional groups (-OH and -NH_2) that explain its higher PL stability.

3.3. Analytical performance of GQD-PAN membranes and dispersed GQD

In order to explore the effect of free chlorine concentration on the PL of GQD-PAN electrospun membranes and water dispersed GQD, we initially selected excitation and emission wavelengths where the analyte did not absorb light. NaClO has an intense absorption band centered at 292 nm and negligible absorbance at wavelengths longer than 370 nm. Therefore, PL spectra were measured exciting at 420 nm, a wavelength where the GQD PL excitation spectrum has a strong band, to avoid any inner-filter effect from NaClO. The sensing performance of GQD-PAN electrospun membranes was investigated in PBS at pH7 because the PL intensity of GQD is pH sensitive and the highest emission corresponds to neutral solutions. On the other hand, pH also determines the form of free chlorine in water (HClO or ClO^-) and in neutral solutions the prevalent form is HClO, with stronger oxidation capability. Fig. 6a shows representative PL spectra of a piece of GQD-PAN membrane immersed in 0.1 M PBS pH 7 recorded immediately (< 10 s) after addition of aliquots of chlorine solution (C_{Cl} = 0 – 1.6 mM). The PL emission of the GQD-PAN membrane at characteristic GQD emission wavelengths (450-550 nm) decreases gradually with increasing chlorine concentration, demonstrating that encapsulated GQD behave as sensitive fluorescent probes for fast chlorine detection. Membrane PL quenching is very pronounced and can be easily detected visually, as illustrated by the photographs in Fig. 6a of several pieces of a GQD-PAN membrane immersed in PBS with different free chlorine concentrations under UV light.

In order to prove that PL quenching arises from encapsulated GQD, the effect of free chlorine concentration in the PL spectra of GQD-free electrospun PAN membranes was investigated. As shown in Fig. S7a (supporting information), the effect of free chlorine in the emission intensity of PAN membranes is negligible (< 5% at the highest concentration, 2.5 mM) compared to the effect on GQD-PAN membranes. Nevertheless, for the calibration plots the background fluorescence of PAN at each chlorine concentration was subtracted from the spectra of GQD-PAN membranes. Moreover, the photostability of GQD-PAN membranes under continuous irradiation at the excitation wavelength (420 nm) in chlorine-free PBS 0.1 M pH 7 was corroborated (supporting information, Fig. S7b), hence ruling out a possible contribution from membrane photodegradation to the observed chlorine-induced PL quenching. PL quenching by strongly oxidizing free chlorine was first reported by Dong et al. [16] for GQD that were surface-passivated by residual citric acid from the pyrolysis synthesis. PL quenching was ascribed to destruction of the surface passivation layer by free chlorine. The GQD luminescent probes used here have been prepared by a different method, known to yield highly crystalline and clean materials without a surface passivation layer. However, PL quenching induced by free chlorine in our non-passivated GQD turned out to be irreversible, as opposed to the reversible PL quenching caused in these GQD by Cr (VI) ion solutions [26]. That is, while reversible GQD PL quenching by Cr (VI) is due to photoinduced electron transfer from GQD to Cr (VI), irreversible GQD PL quenching by chlorine reveals a severe oxidation of GQD that disrupts the integrity of the aromatic sp^2 domains, suppressing totally the emissive electronic transitions. This oxidative mechanism was supported by FTIR spectroscopy, which shows a substantial decrease in the intensity of the aromatic C=C stretch band (1504 cm^{-1}) for GQD samples upon exposure to chlorine (supporting information, Fig. S3A). Comparable changes in FTIR spectra were reported for GQD oxidized by nitric/sulfuric acid mixtures [44]. Furthermore, Raman spectroscopy at 532 nm (supporting information, Fig. S3B) also corroborates a chlorine-induced increase in the amount of defects/sp^3 carbon content, as indicated by the higher I_D/I_G ratio (intensity of the bands at 1372 and 1602 cm^{-1},

respectively) of GQD samples exposed to chlorine (I_D/I_G = 0.98) compared to that of pristine GQD samples (I_D/I_G = 0.84).

As a result of the irreversible oxidation, GQD can only be regarded as one-use "turn-off" fluorescence detection probes. GQD integration into water filtering membranes by electrospinning to produce one-use and low-cost sensing platforms could be an effective approach for real time monitoring of chlorine concentration along the water distribution network. As a proof-of-concept, Fig. 6b shows the linear response of relative PL intensity changes at 478 nm, $(F_0\text{-}F)/F_0$, with free chlorine concentration for the two GQD-PAN electrospun membranes having different fiber diameters (F_0 and F are the PL intensity in absence and presence of free chlorine). Relative PL intensity changes for each concentration were determined as the average value of three replicates. Both membranes exhibit a good linear relationship between the PL quenching ratio at 478 nm and free chlorine concentration in the range from 10 to 600 μM. The PL quenching ratios for both membranes were fitted to the Stern-Volmer equation $(F_0\text{-}F)/F_0 = K_{SV} \times [Cl] + B$, yielding the following Stern-Volmer constants and correlation coefficient values: $K_{SV} = 1.89 \times 10^5\ M^{-1}$ (R^2 = 0.9934, n=10) and $K_{SV} = 1.63 \times 10^5\ M^{-1}$ (R^2 = 0.9903, n=10) for GQD-PAN12 and GQD-PAN10, respectively. These Stern-Volmer constants are 2-3 fold higher than the values previously reported for other GQD as dispersed probes [16], highlighting the excellent performance of GQD encapsulated in PAN membranes for turn-off fluorescence detection of free chlorine. The theoretical detection limits (DL) for free chlorine, calculated as DL = 3 σ/K (where σ is the standard deviation of the blank response and K is the slope of the calibration plot) were 2.0 and 3.7 μM for GQD-PAN12 and GQD-PAN10 respectively. These low detection limits are comparable to those attainable by the widely used DPD (N,N-diethyl-p-phenylenediamine) colorimetric methods [32, 45]. The reproducibility of the detection method, evaluated as the relative standard deviation (R.S.D.) in the detection of 600 μM free chlorine (n=5), was 2.2% and 3.3% for GQD-PAN12 and GQD-PAN10 respectively, indicating an excellent reproducibility with both membranes that is comparable to the precision of standard DPD colorimetric methods [45]. Overall, the very similar analytical response of the two GQD-PAN

membranes indicates the prevalence of GQD concentration effect in the sensing response over morphological differences between both electrospun nanofibrous membranes. Membrane morphology would envisage higher interaction between analyte and sensing probe for membranes with smaller nanofiber diameters (or lower pore volume along the membrane). However, GQD-PAN10 membrane, with lower nanofiber average diameter ($\overline{D}$=595nm) but higher GQD concentration (2.83μg/cm^2) exhibits slightly lower K_{SV} value and higher DL than GQD-PAN12 ([GQD]= 2.00μg/cm^2 and $\overline{D}$=762nm), an analytical response determined by GQD concentration, in agreement with trends observed for water dispersed GQD, as shown in next paragraph.

For comparative purposes, free chlorine detection was also done using GQD as fluorescence probes dispersed in 0.1 M PBS pH 7 aqueous solutions. Fig. 6c shows the PL spectra and photographs under UV light of GQD (0.03 mg/mL) dispersed in PBS pH 7 solutions with different concentrations of free chlorine. In this case, GQD PL emission is totally quenched as there is no background contribution from the PAN matrix. Interestingly, we found that the sensitivity of GQD solutions for free chlorine detection was strongly dependent on GQD concentration, which in turn, determined the PL of the starting (chlorine-free) solution (F_0). This effect is illustrated in Fig. 6d, where the calibration plots of PL quenching ratios vs. chlorine concentration for GQD solutions of different concentrations are shown. Three replicates were measured for each GQD solution. As can be seen, the slope of the calibration plot (that is, sensitivity for chlorine detection) increases with decreasing GQD concentration. As a result, the linear concentration range is shifted to lower concentration as the amount of GQD luminescent probes is decreased. Thus, fitting PL quenching values in the linear concentration range to the Stern-Volmer equation yields the following constants for the different GQD concentrations: $K_{SV} = 3.57 \times 10^4$ M^{-1} ($R^2 = 0.9973$) for 30 μg/mL GQD, $K_{SV} = 5.88 \times 10^4$ M^{-1} ($R^2 = 0.9956$) for 15 μg/mL GQD, $K_{SV} = 1.31 \times 10^5$ M^{-1} ($R^2 = 0.9904$) for 7.5 μg/mL GQD and $K_{SV} = 4.75 \times 10^5$ M^{-1} ($R^2 = 0.9908$) for 1.5 μg/mL GQD. The higher sensitivity of less concentrated GQD solutions leads to lower detection limits for free chlorine, according to the following trends: 80.2, 32.5, 8.8 and 4.7 μM for GQD concentrations of 30, 15, 7.5 and 1.5 μg/mL, respectively. It is worth

indicating that if PL quenching measurements are carried out with GQD solutions placed in a fluorescence cuvette instead of fluorescence plates, the detection test sensitivity is significantly enhanced, attaining detection limits as low as 0.1 μM, comparable to values reported for free chlorine with other GQD solutions [16]. However, the experimental set-up based on the use of fluorescence plates allows direct comparison of the analytical performance of dispersed GQD and GQD-PAN membranes. It is remarkable that GQD-PAN membranes exhibit very high sensitivity (Stern-Volmer constant) and consequently, very low detection limits of free chlorine, even smaller than the lowest ones obtained with GQD as dispersed probes (1.5 μg/mL GQD solutions). That is, encapsulation of GQD in the electrospun PAN membranes enhances the photostability and also the sensing performance of the luminescent nano-probes. These improved features can be attributed to the good dispersion of GQD in the electrospun nanofibers and the unique properties of filtering membranes prepared by electrospinning. The extremely high surface/volume ratio of electrospun nanofibers allows fast interaction between luminescent probes and analyte. Moreover, encapsulation of the GQD probes in the nanofibers prevents aggregation and/or sedimentation phenomena responsible of the PL decay for dispersed GQD. As a result, the analytical response of GQD-PAN nanofibrous membranes outperforms GQD solutions with the best sensing behavior (at low concentrations).

Next, the selectivity of GQD-PAN membranes for chlorine detection was evaluated measuring relative PL intensity changes of several membrane pieces in presence of potentially interfering common ions: Na^+, K^+, Cd^{2+}, Zn^{2+}, Mn^{2+}, Co^{2+}, Mg^{2+}, Ca^{2+}, Pb^{2+}, Fe^{3+}, Ni^{2+}, Cu^{2+}, Fe^{2+}, Ag^+ and Hg^{2+}. Fig. 7a shows average values (n=3) of quenching ratios (F/F_0, where F and F_0 are fluorescence values in presence and absence of each metal ion) for a GQD-PAN10 membrane in 0.1 M PBS pH 7 solution. As can be seen, PL quenching by most tested cations is negligible compared with that induced by chlorine, highlighting the high selectivity of GQD-PAN membranes for free chlorine detection. Only strong oxidants such as $KMnO_4$ or K_2CrO_4 could also quench the PL of GQD-PAN membranes but they are not usually present in natural water samples.

The effect of solution pH value on the membrane sensing response was also investigated. Taking into account that the pH of drinking water typically ranges from 6-8, the membrane response to free chlorine has been evaluated at moderate pH values (Fig.7b). As can be seen, the PL intensity of GQD-PAN membranes (n=5) is not affected by the pH value of chlorine-free buffer solutions in the studied pH range. Only at strongly acidic solutions GQD PL intensity is substantially lowered [36]. However, in presence of 500 μM free chlorine, the magnitude of PL intensity quenching is pH dependent, decreasing sharply in alkaline solutions. As outlined before, this is due to the different oxidation capability of the free chlorine forms existing at each pH value [46]. At pH < 9 free chlorine exists mainly as HClO, which is more oxidizing than the ClO^- anion present in strong alkaline solutions (pH > 9). However, the quenching effect of free chlorine at pH values close to neutral (6-8) is comparable, indicating that GQD-PAN membranes are suitable sensing platforms for drinking water samples. The applicability of the GQD-PAN membranes to detect free chlorine in a real sample was demonstrated using a standard addition method to determine the concentration of free chlorine in local tap water (pH = 7.1). Figure 8 shows relative PL intensity changes at 478 nm of the GQD-PAN10 membrane (n=5) in tap water upon addition of different concentrations of free chlorine in PBS pH 7 solution. From the intercept of the lineal fit with the concentration axis, a concentration of 0.68 ± 0.03 ppm of free chlorine in the tap water sample was estimated, in compliance with Spanish regulation (RD 140-2003) that establishes 1 ppm as the highest free chlorine concentration level in drinking water. For comparison, the concentration was also determined with a commercial digital photometer for free chlorine based on the standard DPD colorimetric method (Hanna Checker Hi 701). The average concentration value for five replicates was 0.64 ± 0.05 ppm, which validates the result obtained with the GQD-PAN membrane. Moreover, the membranes exhibited higher precision than the commercial meter for tap water samples, with R.S.D. of 4.4 % and 7.8% for each method, respectively.

Finally, the stability of the sensing response of GQD-PAN membranes upon storage immersed in 0.1M PBS pH 7 was evaluated. The PL quenching response of the two GQD-PAN membranes in

PBS pH 7 with different chlorine concentrations, just-immersed and after 2 months immersed, are compared in Fig. 9. Plotted $(F_0-F)/F_0$ quenching ratios for both immersion times are the average values of three replicates done with different pieces of each membrane. The PL quenching ratios at each chlorine concentration for the fresh and 2-month soaked membranes are remarkably similar, demonstrating the excellent time stability of wetted GQD-PAN membranes as fluorescence sensing platforms for chlorine detection. In contrast, samples of dispersed GQD in PBS pH7 solutions after 2 months in the fluorescence plate wells had considerable amount of sediment and PL intensity loss (> 35 %). In summary, we have proven that encapsulation of GQD probes in electrospun PAN nanofibrous membranes lead to enhanced phototostability and hence long-term stability of the sensing response for free chlorine detection.

4. Conclusions

PAN nanofibrous membranes containing GQD were produced by one-step electrospinning solutions of both components. The electrospun GQD-PAN membranes exhibited very homogeneous GQD distribution across the membrane surface (300 cm^2), as evidenced by fluorescence microscopy analysis and the uniform PL intensity measured across the whole membrane. The luminescence of both dry and immersed GQD-PAN membranes proved very stable for 2 months and under continuous light irradiation. That is, encapsulation of the GQD in the PAN membrane increased their long-term photostability with respect to the emission of GQD solutions. GQD PL quenching as a result of oxidation by chlorine allowed using GQD-PAN membranes as fluorescence sensing platforms for selective determination of free chlorine in drinking water. Membrane PL quenching by free chlorine was fast (no need of incubation time), very pronounced and easily detected visually under UV light. Fluorimetry detection with GQD-PAN filtration membranes allowed very low detection limits of free chlorine (2 μM), comparable to those attainable by widely used analytical methods and lower than values obtained with GQD solutions. Moreover, the analytical performance of GQD-PAN membranes remained very stable after months immersed in aqueous buffer solution. The irreversible GQD PL quenching makes the sensing platforms single-use but the electrospun filtering membranes could be

used to monitor in real-time chlorine concentration in water distribution networks. In summary, encapsulation of GQD in electrospun PAN filtering membranes enhanced the photostability and sensing performance of the luminescent nano-probes while providing a solid platform more suitable for real sensing applications.

Acknowledgements

Financial support from the Basque Government under the ELKARTEK Program (ACTIMAT project, grant number KK-2015/00094 and KK-2016/00097) is gratefully acknowledged by the authors. Authors also want to thank Dr. Alvaro Colina for his help with Raman spectroscopy.

Captions

Figure 1. (A) TEM image and lateral size distribution of GQD. (B) AFM image and thickness distribution of GQD.

Figure 2. Photographs of PAN electrospun nanofibrous membranes with GQD (A) and without GQD (B). Fluorescence microscopy images under sunlight (C) and UV-vis (450 nm - 494 nm) light (D) from GQD-PAN12 electrospun membrane.

Figure 3. SEM images at different magnifications of GQD-PAN12 (A, E) and GQD-PAN10 (B, F) nanofibrous membranes. Nanofiber diameter distribution of GQD-PAN12 (C) and GQD-PAN10 (D) membranes, as obtained from Image-J software images analysis.

Figure 4. PL emission spectra of water dispersed GQD (7.5 μg/mL), PAN and GQD-PAN membranes (λ_{exc} = 420 nm) as-measured (dashed lines) and corrected by subtracting background emission from PAN (solid lines).

Figure 5. (A) Time evolution of PL intensity at 478 nm (λ_{exc} = 420 nm) of a dry GQD-PAN10 membrane and a GQD aqueous solution (0.015 mg/mL). (B) Time evolution of PL intensity at 478 nm (λ_{exc} = 420 nm) of a dry GQD-PAN12 membrane under irradiation with a fluorescent tube lamp (22W) and photographs of the membrane under UV light. (C) Time evolution of PL intensity at 478 nm (λ_{exc} = 420 nm) of GQD-PAN membranes with immersion time in PBS 0.1 M pH 7.

Figure 6. PL emission spectra of a GQD-PAN10 membrane (A) and a GQD solution (0.03 mg/mL) in 0.1 M PBS pH 7 (C) upon addition of increasing (from top to bottom) chlorine concentrations between 0 and 3 mM. Insets shows photographs under UV light of fluorescence plates containing membranes and GQD solutions with increasing (from left to right) chlorine concentrations. (B) Plot of $(F_0\text{-}F)/F_0$ at 478 nm of GQD-PAN membranes in 0.1 M PBS pH 7 versus chlorine concentration (inset: low concentration range). (D) Plot of $(F_0\text{-}F)/F_0$ at 498 nm of GQD solutions (1.5-30 μg/mL)

in 0.1 M PBS pH 7 versus chlorine concentration. Inset: chlorine-free GQD solutions with increasing (from left to right) concentration under natural and UV light.

Figure 7. (A) Relative fluorescence intensities (F/F_0 at 478 nm) of GQD-PAN10 membrane immersed in 0.1 M PBS pH 7 containing different metal ions at the concentrations indicated in the figure. (B) Fluorescence response of GQD-PAN10 membrane in the absence and presence of 500 μM free chlorine in PBS of different pH values.

Figure 8. PL response at 478 nm of GQD-PAN10 membrane in tap water upon addition of different concentrations of free chlorine in PBS pH 7 solution.

Dr. Virginia Ruiz obtained her PhD in Analytical Chemistry from the University of Burgos (Spain) in 2002 investigating on conducting polymers. In 2010 she joined the Materials Division of IK4-CIDETEC with a Ramón y Cajal Postdoctoral Fellowship, where she has been heading the research unit on carbon nanomaterials until now. Previously she was appointed as senior researcher at Aalto University (5 years), University of Warwick (1 year) and University of Burgos (Juan de la Cierva Postdoctoral Fellowship, 3 years). She has participated in over 25 national and international projects related to applications of conducting polymers, metallic and carbon nanomaterials in functional coatings, sensors, energy conversion and optoelectronics. Lecturer in MSc and PhD in Chemistry programmes, she has also supervised several MSc theses and one PhD thesis in the field of carbon nanomaterials for fuel cells. She is co-author of over 75 scientific papers in SCI journals, 1 invited tutorial review, 2 book chapters and 1 patent related to nanomaterials, polymer chemistry, electrochemistry, sensors and energy conversion.

Mrs. Ana Pérez-Marquez. Chemical Engineer (UPV-EHU, Bilbao) in 2008 and Master of Innovation and Technology management (Deusto Business School, San Sebastián) in 2009. She worked in educative cooperation in Degremont between 2007 and 2008 in the field of water treatment plants. In 2008, she joined the department of ceramic materials of Inasmet as junior researcher and worked in the field of nanomaterials focusing on the development of nanofibers based on electrospinning process. At present, she is a researcher in the Aerospace department within the Industry and Transport Division of Tecnalia. Her research interests are in the field of synthesis and manufacture of micro and nano-structured materials by electrospinning technology for different applications which included air filtration, veils for composite materials to reinforce its mechanical properties against impacts, membranes for water decontamination, development of more efficient and selective resistive sensors for chemical substances and gases detection.

Mr. Jon Maudes. Technical Engineer in Electronics (UPV-EHU, San Sebastián) in 1999, Master of Smart Materials (UPV-EHU, Bilbao) in 2007 and Industrial Engineer (ETSII-UNED, Madrid) in 2013. He joined Inasmet in 2002 as junior researcher and worked in the field of metal matrix composite materials focusing on mechanical properties using foundry techniques. In 2007 he joined the department of ceramic materials and powder metallurgy and worked in metallic and ceramic materials focusing on composite materials with high thermal dissipation capability using powder metallurgy processes. Since 2011, he is a researcher in the Aerospace department within the Industry and Transport Division of Tecnalia. He is currently involved in the development and characterization of piezoelectric and nanostructured materials. He has participated in over 25 national and international projects.

Dr. Hans-Jürgen Grande works as the Director of Research & Technology at CIDETEC. He accumulates over 20 years extensive experience in advising, organizing and managing research, innovation, technology transfer and international projects. He received his Ph.D. degree from the University of the Basque Country within the interpretation and theoretical modelling of electrically stimulated conformational relaxation processes in electroactive polymer thin films, and its application to advanced microelectronics. He has been author or co-author of over 160 scientific publications (h index: over 20) and 23 patent families (11 of them currently active).

Dr. Nieves Murillo received her PhD in Physical of Material at the University of the Basque Country (Spain) in 1997. During her thesis she was awarded with Marie Curie Fellowship at the IMEM-CNR Institute in Parma (Italy) and developed part of her research activities in the CSIC Madrid (Spain). She has held post-doctoral

position at the Max-Planck Institute in Stuttgart (Germany). Since then, she was awarded with a Ramon y Cajal Fellow at Cidetec with successful assessment of I3 evaluation. Her research fields are focused in two main areas: sensor and actuator development based on smart materials, including optical, piezoelectric, magnetic and superconducting, including materials design, fabrication and application development. She has participated in over 40 international and national projects, she is co-author of over 50 scientific publications, including a book chapter. Her citation level is over 280. She has been member of organizing committees of three International conferences. She has imparted more than 10 invited talks at international events.

Figure 9. (A) Time stability of immersed GQD-PAN membranes as sensing platforms: plot of $(F_0-F)/F_0$ at 478 nm versus chlorine concentration of GQD-PAN10 (A) and GQD-PAN12 (B) membranes as-prepared and after 2 months immersed in 0.1 M PBS pH 7.

References

References

[1] S.N. Baker, G.A. Baker, Luminescent carbon nanodots: emergent nanolights, Angew. Chem. Int. Ed. 49 (2010) 6726-6744.

[2] M.O. Dekaliuk, O. Viagin, Y.V. Malyukin, A.P. Demchenko, Fluorescent carbon nanomaterials: “quantum dots” or nanoclusters?, Phys. Chem. Chem. Phys. 16 (2014) 16075-16084.

[3] M. Bacon, S. J. Bradley, T. Nann, Graphene quantum dots, Part. Part. Syst. Charact. 31 (2014) 415-428.

[4] X.T. Zheng, A. Ananthanarayanan, K.Q. Luo, P. Chen, Glowing graphene quantum dots and carbon dots: properties, syntheses and biological applications, Small 11 (2015) 1620–1636.

[5] S.H. Song, M.H. Jang, J. Chung, S.H. Jin, B.H. Kim, S.H. Hur et al., Highly efficient light-emitting diode of graphene quantum dots fabricated from graphite intercalation compounds, Adv. Opt. Mater. 2 (2014) 1016–1023.

[6] C.X. Guo, H.B. Yang, Z.M. Sheng, Z.S. Lu, Q.L. Song, C.M. Li, Layered graphene/quantum dots for photovoltaic devices, Angew. Chem. Int. Ed. 49 (2010) 3014-3017.

[7] Z. Zhang, J. Zhang, N. Chen, L. Qu, Graphene quantum dots: an emerging material for energy-related applications and beyond, Energy Environ. Sci. 5 (2012) 8869-8890.

[8] K.A.S. Fernando, S. Sahu, Y. Liu, W.K. Lewis, E.A. Guliants, A. Jafariyan et al., Carbon quantum dots and applications in photocatalytic energy conversion, ACS Appl. Mater. Inter. 7 (2015) 8363-8376.

[9] H. Sun, L. Wu, W. Wei, X. Qu, Recent advances in graphene quantum dots for sensing, Materials Today 16 (2013) 433–442.

[10] S. Benitez-Martinez, M. Valcarcel, Graphene quantum dots in analytical science, TRAC-Trend Anal. Chem. 72 (2015) 93–113.

[11] L. Lin, M. Rong, F. Luo, D. Chen, Y. Wang, X. Chen, Luminescent graphene quantum dots as new fluorescent materials for environmental and biological applications, TRAC-Trend Anal. Chem. 54 (2014) 83–102.

[12] J.J. Huang, M.Z. Rong, M.Q. Zhang, Preparation of graphene oxide and polymer-like quantum dots and their one- and two-photon induced fluorescence properties, Phys. Chem. Chem. Phys. 18 (2016) 4800-4806.

[13] T.V. Tam, N.B. Trung, H.R. Kim, J.S. Chung, W.M. Choi, One-pot synthesis of N-doped graphene quantum dots as a fluorescent sensing platform for Fe^{3+} ions detection, Sens. Actuators B-Chem. 202 (2014) 568–573.

[14] F. Wang, Z. Gu, W. Lei, W. Wang, X. Xia, Q. Hao, Graphene quantum dots as a fluorescent sensing platform for highly efficient detection of copper (II) ions, Sens. Actuators B-Chem. 190 (2014) 516-522.

[15] H. Huang, L. Liao, X. Xu, M. Zou, F. Liu, N. Li, The electron-transfer based interaction between transition metal ions and photoluminescent graphene quantum dots (GQDs): a platform for metal ion sensing, Talanta 117 (2013) 152–157.

[16] Y. Dong, G. Li, N. Zhou, R. Wang, Y. Chi, G. Chen, Graphene quantum dot as a green and facile sensor for free chlorine in drinking water, Anal. Chem. 84 (2012) 8378–8382.

[17] Z. Qu, X. Zhou, L. Gu, R. Lan, D. Sun, D. Yu et al., Boronic acid functionalized graphene quantum dots as fluorescent probe for selective and sensitive glucose determination in microdialysate, Chem. Commun. 49 (2013) 9830–9832.

[18] Y. Li, L. Zhang, J. Huang, R. Liang, J. Qiu, Fluorescent graphene quantum dots with a boronic acid appended bipyridinium salt to sense monosaccharides in aqueous solution, Chem. Commun. 49 (2013) 5180–5182.

[19] L. Li, G. Wu, T. Hong, Z. Yin, D. Sun, E.S. Abdel-Halim et al., Graphene quantum dots as fluorescence probes for turn-off sensing of melamine in the presence of Hg^{2+}, ACS Appl. Mater. Inter. 6 (2014) 2858–2764.

[20] Z. Zeng, D. Yu, Z. He, J. Liu, F.X. Xiao, Y. Zhang et al., Graphene oxide quantum dots covalently functionalized PVDF membrane with significantly-enhanced bactericidal and antibiofouling performances, Sci. Rep. 6 (2016) 20142.

[21] C. Zhang, K. Wei, W.Zhang, Y. Bai, Y. Sun, J. Gu, Graphene oxide quantum dots incorporated thin film nanocomposite membrane with high flux and antifouling properties for low-pressure nanofiltration, ACS Appl. Mater. Inter. 9 (2017) 11082–11094.

[22] X. Song, Q. Zhou, T. Zhang, H. Xu, Z. Wang, Pressure-assisted preparation of graphene oxide quantum dot incorporated reverse osmosis membranes: antifouling and chlorine resistance potentials, J. Mater. Chem. A. 4 (2016) 16896-16905.

[23] S. Chen , Y. Song, F. Shi, Y. Liu, Q. Ma, Sensitive detection of picric acid based on creatinine-capped solid film assembled by nitrogen-doped graphene quantum dots and chitosan. Sens. Actuators B-Chem. 231 (2016) 634–640.

[24] W. Zhang, J. Gan, Synthesis of blue-photoluminescent graphene quantum dots/polystyrenic anion-exchange resin for Fe(III) detection, Appl. Surf. Sci. 372 (2016) 145–151.

[25] S. Li, S. Zhou, H.Xu, L. Xiao, Y. Wang, H. Shen et al., Luminescent properties and sensing performance of a carbon quantum dot encapsulated mesoporous silica/polyacrylonitrile electrospun nanofibrous membrane, J. Mater. Sci. 51 (2016) 6801-6811.

[26] P.M. Carrasco, I. García, L. Yate, R. Tena-Zaera, G. Cabanero, H.J. Grande, V. Ruiz, Graphene quantum dot membranes as fluorescent sensing platforms for Cr (VI) detection, Carbon 109 (2016) 658-665.

[27] N. Bhardwaj, S.C. Kundu, Electrospinning: a fascinating fiber fabrication technique, Biotechnol. Adv. 28 (2010) 325–347.

[28] S. Mohammadzadehmoghadam, Y. Dong, S. Barbhuiya, L. Guo, D. Liu, R. Umer, X. Qi, Y. Tang, Electrospinning: current status and future trends, in: S. Fakiro (Ed.), Nano-size Polymers, Springer International Publishing, Switzerland, 2016, pp 89-154.

[29] P. Zhang, X. Zhao, Y. Ji, Z. Ouyang, X. Wen, J Li et al. Electrospinning graphene quantum dots into a nanofibrous membrane for dual-purpose fluorescent and electrochemical biosensors, J. Mater. Chem. B 3 (2015) 2487-2496.

[30] S. D. Richardson, C. Postigo, Drinking water disinfection by-products, in: Emerging Organic Contaminants and Human Health, Springer, Berlin, Germany, 2012; pp 93−137.

[31] J. Rodriguez, J. B. Sérodes, Assessing empirical linear and non-linear modelling of residual chlorine in urban drinking water systems, Environ. Modell. Softw. 14 (1998) 93–102.

[32] Standard methods for the examination of water and wastewater, 16th ed., APHA, AWWA, WPCF, Washington, D.C., 1985.

[33] M. Murata, T. A Ivandini, M. Shibata, S. Nomura, A. Fujishima, Y. Einaga, Electrochemical detection of free chlorine at highly boron-doped diamond electrodes, J. Electroanal. Chem. 612 (2008) 29−36.

[34] J. Sullivan, M. Douek, Determination of inorganic chlorine species in kraft mill bleach effluents by ion chromatography, J. Chromatogr. A 804 (1998) 113−121.

[35] https://imagej.nih.gov/ij/

[36] L. Wang, Y. Wang, T. Xu, H. Liao, C. Yao, Y. Liu, et al., Gram-scale synthesis of single-crystalline graphene quantum dots with superior optical properties, Nat. Commun. 5 (2014) 5357.

[37] V. Ruiz, L. Yate, I. García, G. Cabanero, H.J. Grande, Tuning the antioxidant activity of graphene quantum dots: protective nanomaterials against dye decoloration, Carbon 116 (2017) 366-374.

[38] D. F. Báez, H. Pardo, I. Laborda, J. F. Marco, C. Yáñez, S. Bollo, Reduced graphene oxides: influence of the reduction method on the electrocatalytic effect towards nucleic acid oxidation, Nanomaterials 7 (2017) 168-182.

[39] M.A. Sk, A. Ananthanarayanan, L. Huang, K. H. Lim, P. Chen, Revealing the tunable photoluminescence properties of graphene quantum dots, J. Mater. Chem. C 2 (2014) 6954-6960.

[40] S.D. Choudhury, J.M. Chethodil, P. M. Gharat, P. K. Praseetha, H. Pal, pH elicited luminescence functionalities of carbon dots: mechanistic insights, J. Phys. Chem. Lett. 8 (2017) 1389–1395.

[41] P. Deb, T. Haldar, S. M. Kashid, S. Banerjee, S. Chakrabarty, S. Bagchi, Correlating nitrile IR frequencies to local electrostatics quantifies noncovalent interactions of peptides and proteins, J. Phys. Chem. B 120 (2016) 4034-4046.

[42] Q. A. Acton in Nitriles: Advances in Research and Application, Scholarly Editions, Atlanta, Georgia, 2011.

[43] N. Wang, K. Burugapalli, W. Song, J. Halls, F. Moussy, Y. Zheng et al., Tailored fibro-porous structure of electrospun polyurethane membranes, their size-dependent properties and transmembrane glucose diffusion, J. Membr. Sci. 427 (2013) 207–217.

[44] M. H. Jang, H. D. Ha, E. S. Lee, F. Liu, Y. H. Kim, T. S. Seo et al., Is the chain of oxidation and reduction process reversible in luminescent graphene quantum dots? Small 11 (2015) 3773–3781.

[45] D. L. Harp, Current Technology of Chlorine Analysis for Water and Wastewater, in: Technical Information Series Booklet No.17, Hach Company, USA, 2002.

[46] T. Aoki, M. Munemorl, Continuous flow determination of free chlorine in water, Anal. Chem. 55 (1983) 209-212.Figure Caption

Figr-1 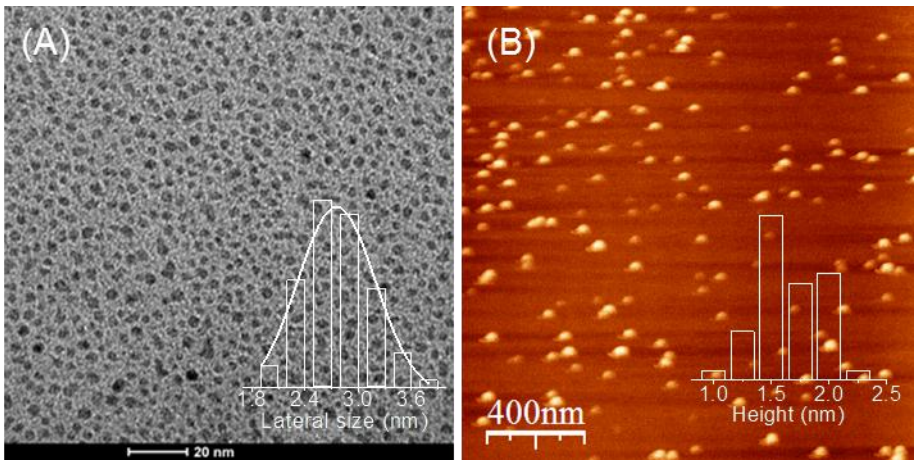

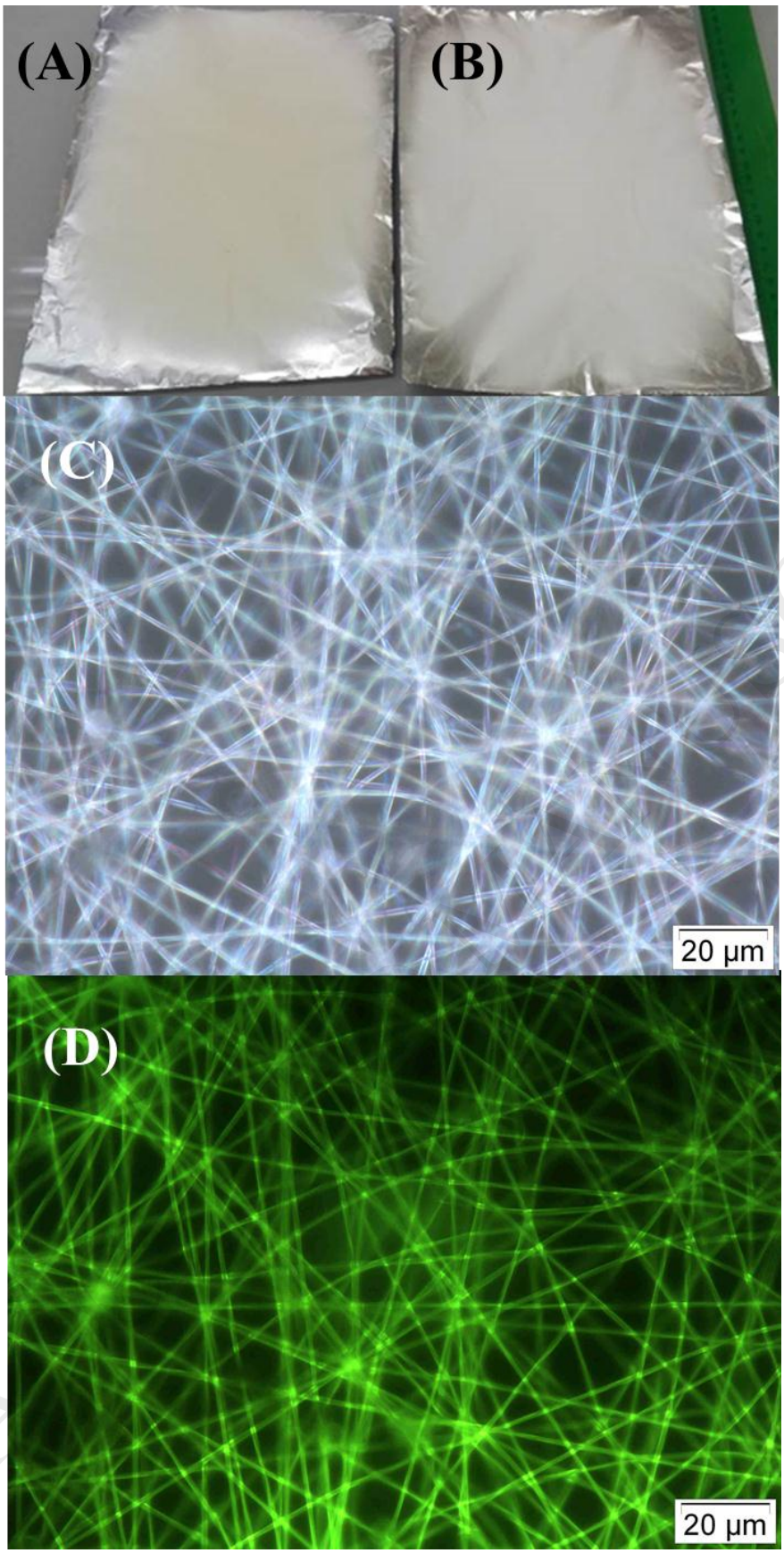

Figr-2

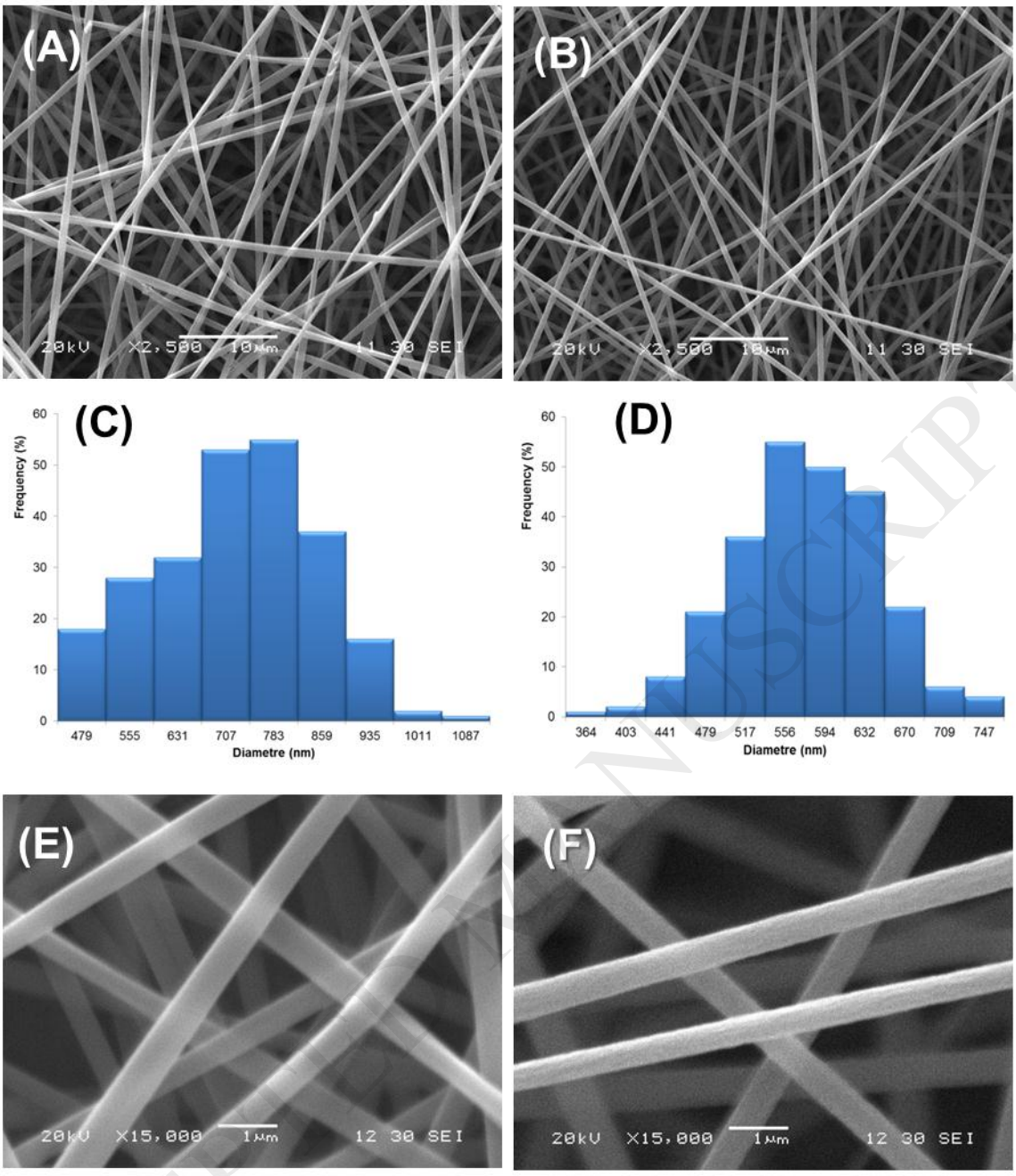

Figr-3

Figr-4

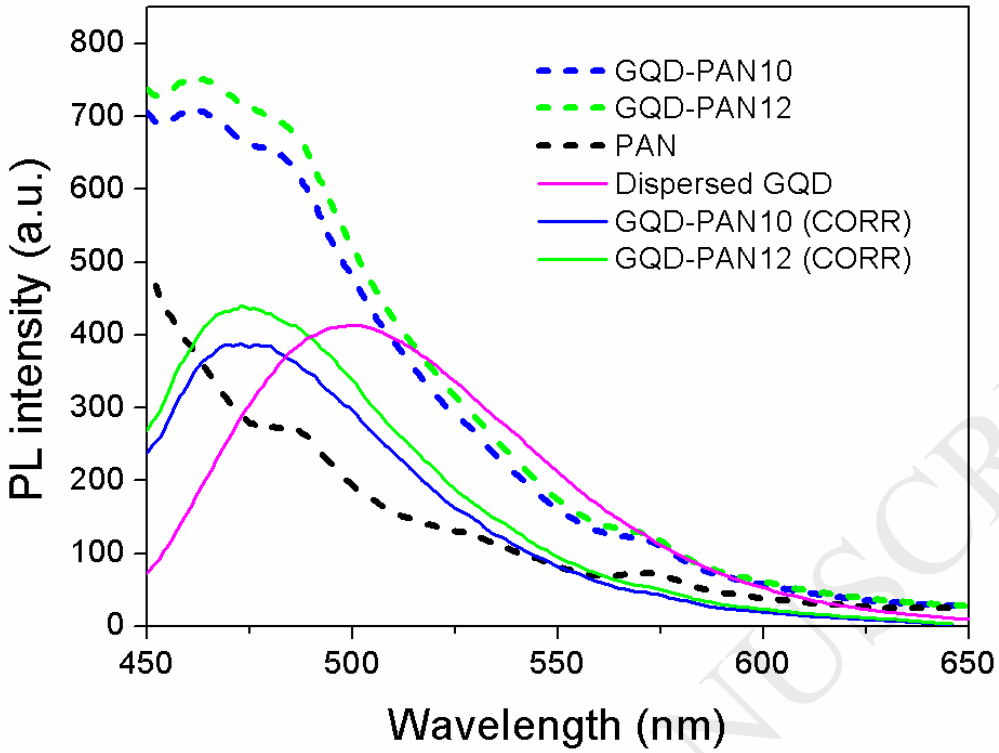

Figr-5

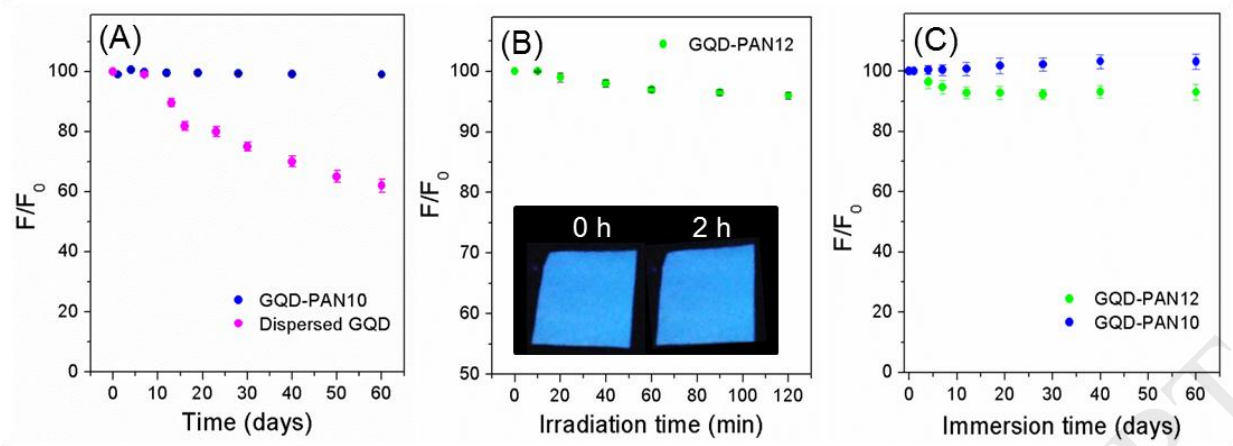

Figr-6

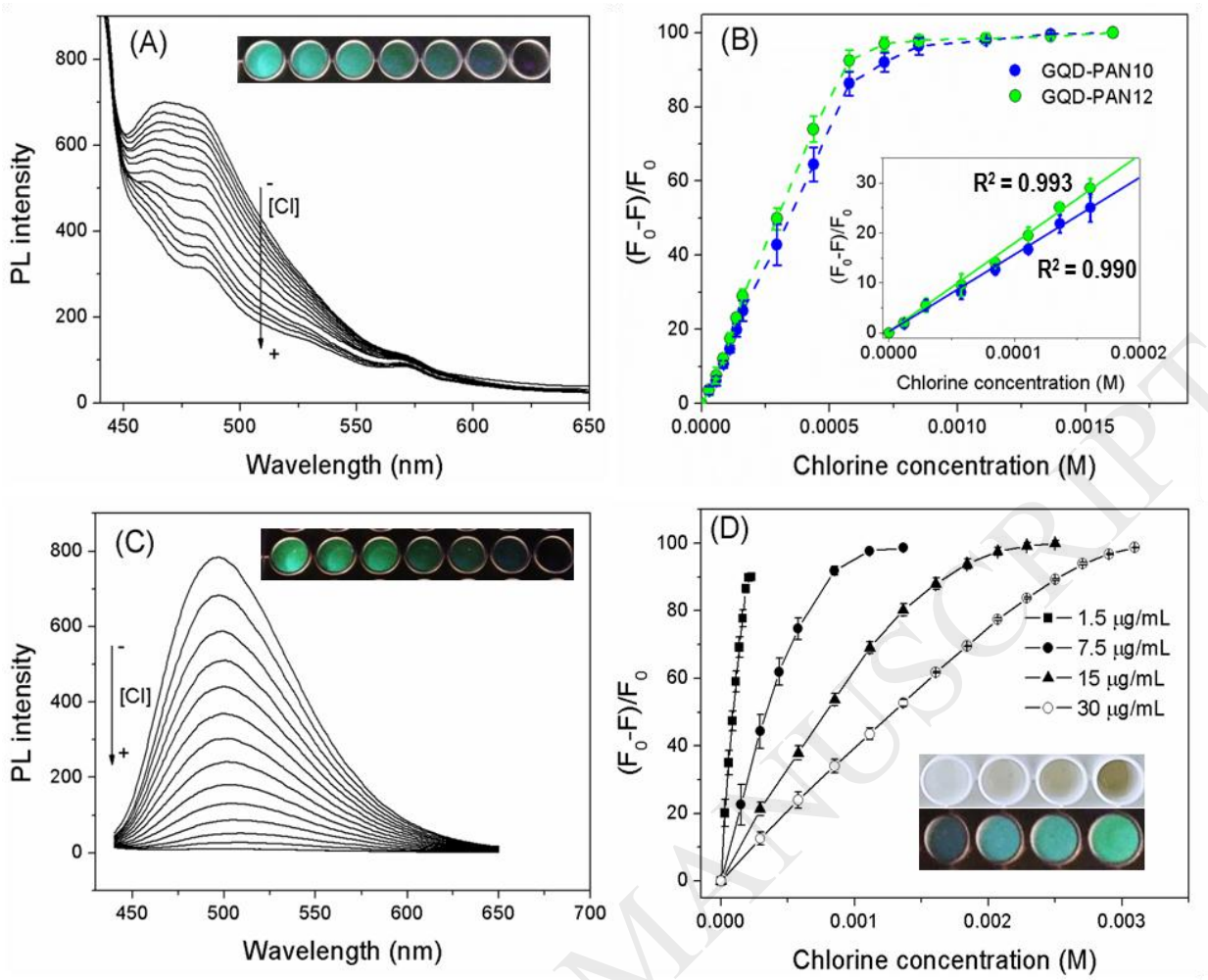

Figr-7

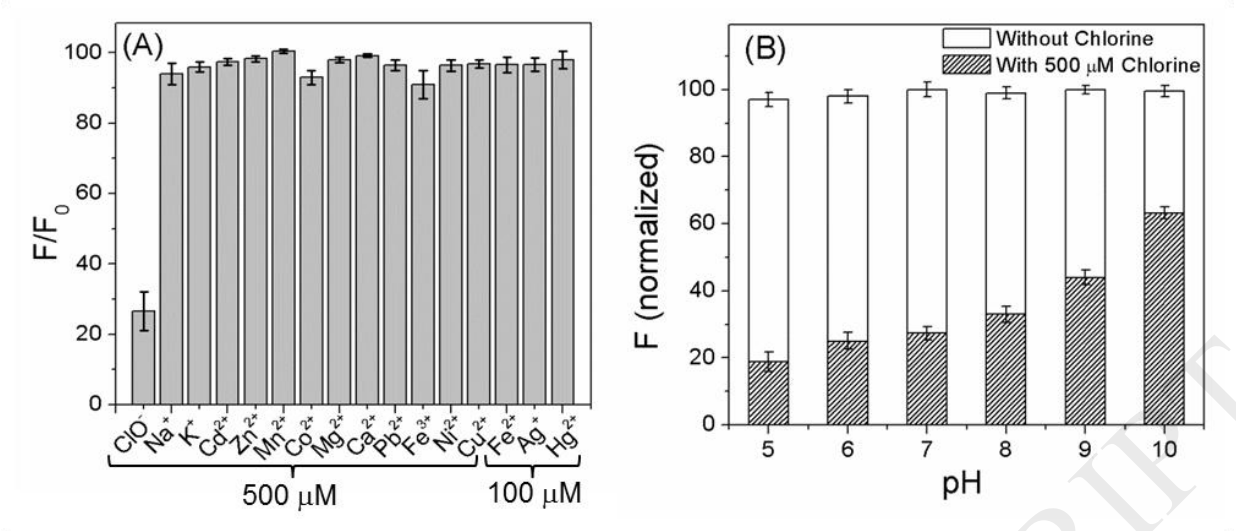

Figr-8

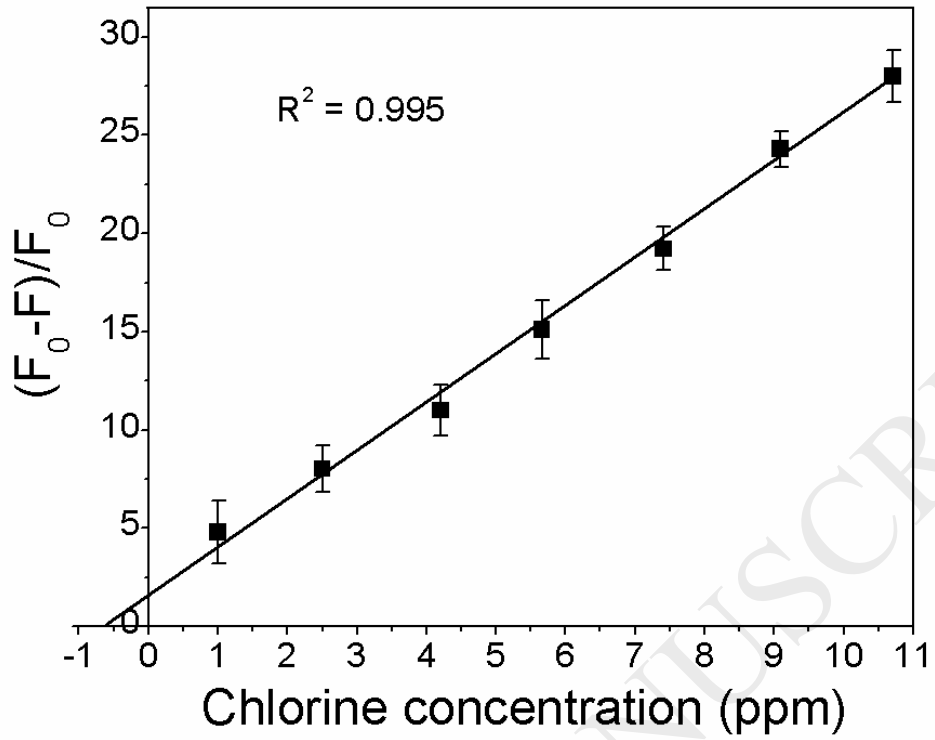

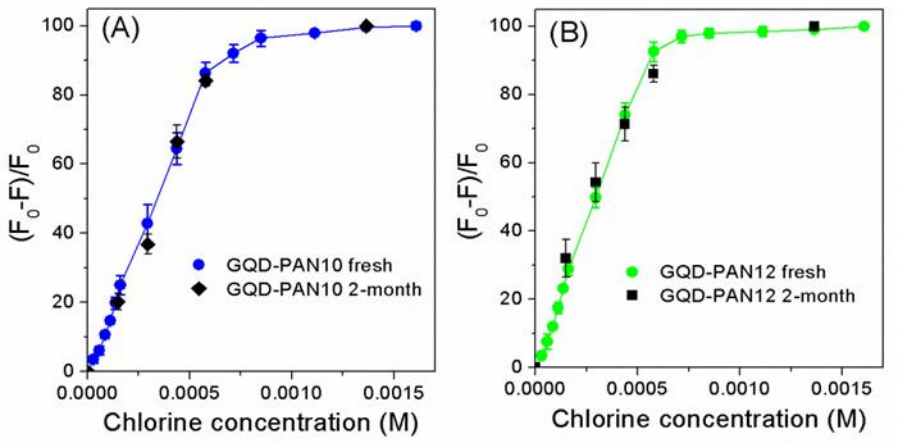

Figr-9